Mesoscale eddies in the northeastern Pacific tropical-subtropical transition zone: Statistical characterization from satellite altimetry

J. A. Kurczyn, Emilio Beier, Miguel F. Lavín, Alexis Chaigneau

Mesoscale eddies in the northeastern Pacific tropical-subtropical transition zone: Statistical characterization from satellite altimetry

J. A. Kurczyn,[1] E. Beier,[2] M. F. Lavín,[1] and A. Chaigneau[3]

Received 10 February 2012; revised 24 August 2012; accepted 6 September 2012; published 24 October 2012.

[1] Mesoscale eddies in the northeastern Pacific tropical-subtropical transition zone (16°N–30°N; 130°W–102°W) are analyzed using nearly 18 years of satellite altimetry and an automated eddy-identification algorithm. Eddies that lasted more than 10 weeks are described based on the analysis of 465 anticyclonic and 529 cyclonic eddy trajectories. We found three near-coastal eddy-prolific areas: (1) Punta Eugenia, (2) Cabo San Lucas, and (3) Cabo Corrientes. These three areas are located in places where the coastal morphology changes abruptly and strong surface current intensification occurs at some phase of the seasonal cycle. Although mesoscale eddies in these areas have been previously reported, this study provides their first statistically supported characterization. Punta Eugenia showed the highest eddy production (with more cyclones generated), followed by Cabo Corrientes (also with more cyclones) and Cabo San Lucas (with more anticyclones). Cabo Corrientes eddies showed the highest mean values in propagation speed, swirling speed and eddy kinetic energy, whereas Punta Eugenia eddies showed the lowest values. Cyclonic eddies increased their distance traveled and duration from south to north; in contrast anticyclonic eddies increased from north to south. In average, anticyclones tend to travel faster than cyclones in all the subregions. These long-lived eddies were mainly nonlinear and therefore can redistribute coastal waters relatively far into the open ocean. The peaks in the seasonal signal of eddy generation can be associated with the peaks in the strength of the offshore currents and/or in the Coastal Upwelling Index. No clear relationship could be established between El Niño events and eddy generation.

Citation: Kurczyn, J. A., E. Beier, M. F. Lavín, and A. Chaigneau (2012), Mesoscale eddies in the northeastern Pacific tropical-subtropical transition zone: Statistical characterization from satellite altimetry, *J. Geophys. Res.*, *117*, C10021, doi:10.1029/2012JC007970.

1. Introduction

[2] The northeastern (NE) Pacific tropical-subtropical transition zone, located at 16°N–30°N and 130°W–102°W (Figure 1), is the region of confluence of two large oceanic currents: the equatorward California Current, which carries relatively cold and dense water of subarctic origin, and the near-surface poleward Mexican Coastal Current, which brings relatively warm and light water of tropical origin. Approximately off the tip of the Baja California peninsula the California Current separates into two branches, one feeding the westward North Equatorial Current, while the other continues equatorward along the Mexican coast. The latter branch, which we shall call the tropical branch of the California Current, is particularly evident during boreal spring and winter (Figures 1a and 1d) [*Kessler*, 2006; *Godínez et al.*, 2010]. In contrast, the poleward Mexican Coastal Current is particularly evident in summer (Figure 1b) [*Lavín et al.*, 2006; *Kessler*, 2006].

[3] The main motivation of this study is that in addition to this large-scale circulation, the NE Pacific tropical-subtropical transition zone is also characterized by a relatively intense mesoscale activity, which has not been studied sufficiently. *Godínez et al.* [2010] found that mesoscale variability of the surface circulation is as important as the seasonal and interannual variability, accounting for 30% of the local explained variance. Although many features of this eddy activity are still unknown, sparse hydrographic observations have provided some information on the typical characteristics of a few eddies [*Lynn and Simpson*, 1987; *Simpson and Lynn*, 1990; *Durazo and Baumgartner*, 2002; *Soto-Mardones et al.*, 2004; *Lavín et al.*, 2006; *Jerónimo and Gómez-Valdés*, 2007]. Numerical simulations have also contributed to better understand the mesoscale dynamics of the region and the physical forcing involved in near-coastal eddy generation. For instance, mesoscale eddies can be formed through baroclinic instabilities of the near-coastal

[1]Departamento de Oceanografía Física, CICESE, Ensenada, Mexico.
[2]CICESE Unidad La Paz, La Paz, Mexico.
[3]Laboratoire d'Études en Géophysique et Océanographie Spatiale, UMR 5566, IRD, CNRS, CNES, UPS, Toulouse, France.

Corresponding author: J. A. Kurczyn, Departamento de Oceanografía Física, CICESE, Carretera Ensenada-Tijuana No. 3918, Zona Playitas, C.P. 22860 Ensenada, Baja California, México. (alexk@cicese.edu.mx)

0148-0227/12/2012JC007970

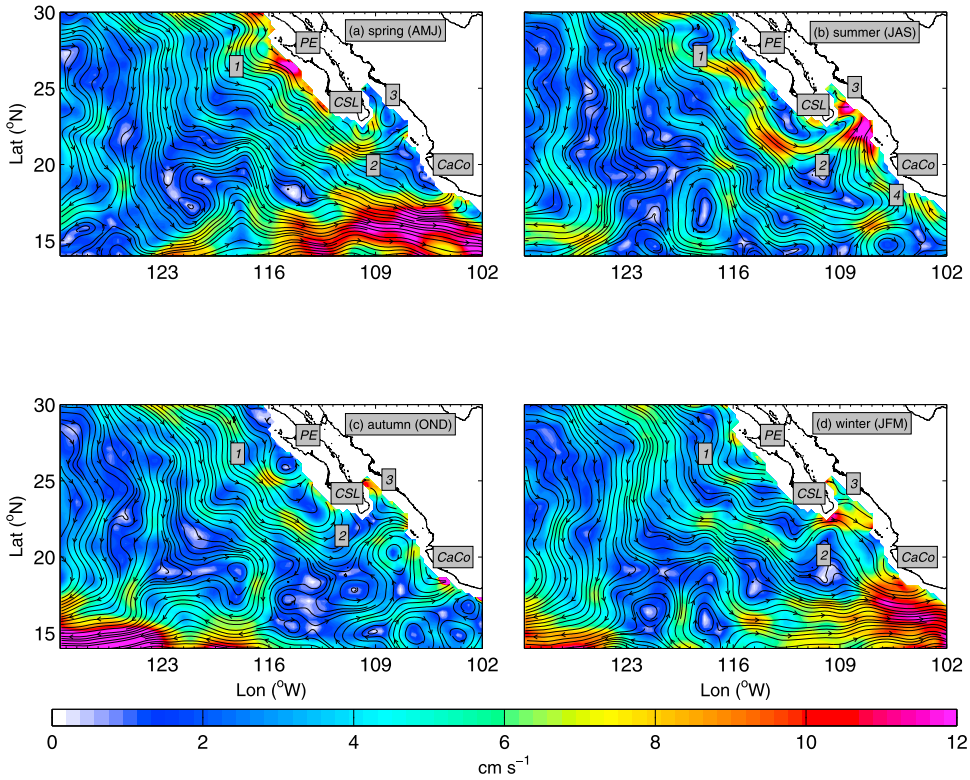

Figure 1. Climatologic geostrophic flow (cm/s) for (a) spring, (b) summer, (c) autumn and (d) winter, obtained as the sum of SLA climatology and the mean geopotential anomalies referred to WOA01 1027 kg/m^{3}isopycnal, showing (1) the California Current, (2) the tropical branch of the California Current, (3) the Gulf of California Current and (4) the Mexican Coastal Current. Subregion areas: PE for Punta Eugenia, CSL for Cabo San Lucas and CaCo for Cabo Corrientes.

currents [*Pantoja et al.*, 2012], interaction of the large-scale circulation with the bottom topography [*Kurian et al.*, 2011], local wind-forcing [*Pares-Sierra et al.*, 1993], or coastally trapped waves of equatorial origin [*Zamudio et al.*, 2001, 2007]. All these studies have also revealed the propagation of eddies over large distances toward the open ocean.

[4] The use of sea level anomaly (SLA) data acquired from satellite altimeters in conjunction with automated eddy detection methods have revolutionized the study of mesoscale eddy activity worldwide, providing robust statistical results based on a great number of eddy observations. One of the most commonly used automated methods is the one based on the Okubo-Weiss parameter [*Okubo*, 1970; *Weiss*, 1991]. Although widely used [*Morrow et al.*, 2004; *Chelton et al.*, 2007; *Henson and Thomas*, 2008; *Kurian et al.*, 2011]. This method is now known to have several limitations [*Haller*, 2005; *Sadarjoen and Post*, 2000; *Chaigneau et al.*, 2008; *Nencioli et al.*, 2010; *Chelton et al.*, 2011; *Souza et al.*, 2011]: (i) a tendency to overestimate eddy abundance by identifying "false eddies," (ii) the need to define a threshold value that depends on regional characteristics of the flow and can introduce bias in eddy detection; and (iii) errors of the SLA field that are amplified by the second derivatives used to estimate the Okubo-Weiss parameter. Recently, other automated methods have been developed and proven to perform much better than the Okubo-Weiss parameter: the Winding-angle method [*Sadarjoen and Post*, 2000; *Chaigneau et al.*, 2008], the Vector geometry-based method [*Nencioli et al.*, 2010] and the Sea Level Anomaly Based method (SLA-B) [*Chaigneau et al.*, 2009; *Chelton et al.*, 2011].

[5] Although previous studies have revealed some of the major features of mesoscale eddies in various sites of the World Ocean, a detailed description of the main eddy characteristics (diameters, propagation speeds, space and time generation, etc.) in the NE Pacific tropical-subtropical transition zone is still lacking. Thus, the main goal of this study is to provide a robust statistical analysis of the main eddy properties in the NE Pacific tropical-subtropical zone, using nearly 18 years of altimetry SLA data and the SLA-B method to automatically detect eddies. In particular, we aim to identify the main eddy generation areas and their subsequent propagation and to highlight differences in eddy properties between several subregions. We also investigate the seasonal and interannual variability of eddy generation and the relationship between the observed variability and some physical forcings. This study provides important results that enhanced our comprehension of the mesoscale dynamics in the study region, as well as essential metrics to be confronted to numerical models, and to help in the interpretation of hydrological data sets.

2. Data and Methods

2.1. Satellite Altimetry Data and Geostrophic Velocity Computations

[6] The altimeter data analyzed in this study are the high-resolution sea level anomalies distributed by *Ssalto*/*Duacs* at

Table 1. Statistical Analysis (Mean ± One Standard Deviation) of Eddy Characteristics From 1992 to 2010, for the Whole Study Region, and for the Three Coastal Subregions[a]

Regions	Total Eddy Count	Total Eddy Generation	Distance Traveled (km)	Duration (days)	Diameter (km)	Propagation Speed (cm/s)	Swirling Speed (cm/s)	EKE (cm^2/s^2)	Amplitude (cm)	Nonlinear Parameter Value
Whole Region	*8848*	*465*	*649 ± 430*	*133 ± 72*	*205 ± 33*	*5.4 ± 2*	*10.9 ± 4*	*78 ± 60*	*5 ± 2*	*2.4 ± 1*
			(2505,102)	*(518,70)*	*(560,80)*	*(79,0)*	*(33,4)*	*(620,8)*	*(24,1)*	*(9,0)*
	11579	529	687 ± 442	153 ± 96	206 ± 34	5.3 ± 2	11.5 ± 4	85.2 ± 67	−5 ± 3	2.4 ± 1
			(3104,63)	(651,70)	(463,64)	(84,0)	(52,3)	(1436,6)	(−24, −1)	(11,0)
Punta Eugenia	*1591*	*74*	*608 ± 383*	*151 ± 94*	*185 ± 28*	*4.6 ± 2*	*9.6 ± 3*	*59 ± 35*	*5 ± 2*	*2.3 ± 1*
			(2093,179)	*(518,70)*	*(405,84)*	*(67,0)*	*(22,4)*	*(269,9)*	*(12,2)*	*(6,0)*
	2944	89	811 ± 464	232 ± 128	190 ± 29	3.9 ± 1	12.0 ± 4	92 ± 61	−7 ± 3	2.8 ± 1
			(2197,140)	(651,70)	(422,78)	(55,0)	(31,5)	(513,13)	(−23, −1)	(8,0)
Cabo San Lucas	*1347*	*65*	*658 ± 459*	*145 ± 85*	*186 ± 27*	*4.9 ± 2*	*11.2 ± 4*	*90 ± 58*	*5 ± 2*	*2.7 ± 1*
			(2261,141)	*(406,70)*	*(427,82)*	*(45,0)*	*(27,5)*	*(414,14)*	*(15,1)*	*(6,0)*
	1283	49	740 ± 604	183 ± 126	190 ± 28	4.4 ± 1	12.9 ± 4	105 ± 76	−6 ± 3	2.7 ± 1
			(3104,63)	(595,70)	(440,91)	(46,0)	(38,6)	(766,18)	(−20, −2)	(9,0)
Cabo Corrientes	*1319*	*58*	*854 ± 495*	*159 ± 93*	*208 ± 26*	*6.3 ± 2*	*13.9 ± 4*	*122 ± 81*	*6 ± 3*	*2.9 ± 1*
			(2204,237)	*(406,70)*	*(465,84)*	*(62,0)*	*(33,5)*	*(620,16)*	*(24,2)*	*(9,0)*
	1300	67	704 ± 433	136 ± 81	205 ± 35	5.9 ± 2	13.0 ± 4	108 ± 88	−5 ± 3	2.6 ± 1
			(2599,209	(581,70)	(424,67)	(58,0)	(52,3)	(1436,6)	(−23, −2)	(11,0)

[a]Italicized values are AEs, maximum and minimum values are in brackets.

7-day intervals on a 1/3° Mercator grid, objectively interpolated onto a uniform 1/4° grid and referenced to a relative 7-year mean (1993–1999) (http://www.aviso.oceanobs.com) [*Ducet et al.*, 2000; *Le Traon et al.*, 2003]. Our data extends from October 1992 to October 2010, and represent the updated multimission gridded product referred by AVISO (Archiving Validation and Interpretation of Satellite Oceanographic Data) as the "Delay Time maps of sea level anomaly (DT-mslaupd)." It merges measurements from between 2 to 4 simultaneously operating altimeters, except between December 1993 and March 1995 when only one altimeter was available. During this period, the eddy kinetic energy (EKE) levels decreased by around 30% for the entire ocean [*Ducet et al.*, 2000]. The AVISO data set is ideally suited to resolve SLA scales of O(100 km) but fails to resolve small scale features having a diameter of ∼10–50 km [*Chelton et al.*, 2011]. One of the limitations of this data set is the loss of accuracy in near coastal regions due to the effects induced by land, both in the satellite measurements and in the modeling of some of the geophysical corrections applied to the measurements. Thus, in general the satellite altimetry product used in this study is reliable only a few tens of km away from the coast.

[7] In order to reduce (1) potential errors in the data arising from uncertainty in the geoid [*Strub and James*, 2002; *Willis et al.*, 2004] and (2) the large-scale effect of the annual steric variations which can partially mask the signature of eddies [*Willis et al.*, 2004; *Guerrero et al.*, 2004; *Henson and Thomas*, 2008; *Chelton et al.*, 2007, 2011], both the long-term temporal mean and the annual cycle of the SLA were removed from the AVISO SLA time series at each grid-cell. The zonal and meridional components (u and v, respectively) of the surface geostrophic velocity were estimated using the classic relations:

$$u = -\frac{g}{f}\frac{\partial \eta}{\partial y}, \quad v = \frac{g}{f}\frac{\partial \eta}{\partial x},$$

where g is the gravitational acceleration, f is the Coriolis parameter, η is the slightly filtered SLA, and ∂x and ∂y are eastward and northward distances.

2.2. Eddy Detection Algorithm

[8] To automatically identify mesoscale features from SLA maps we used the SLA-B method, which is a slightly modified version of the winding-angle method introduced by *Sadarjoen and Post* [2000]. It is based on the geometric properties of the flow under the assumption that vortices are characterized by roughly circular streamlines around their cores [*Robinson*, 1991]. Under the geostrophic approximation, closed streamlines approximately correspond to closed SLA contours. As detailed by *Chaigneau et al.* [2009], this eddy-detection algorithm first searches for eddy centers associated with local SLA absolute maxima in a moving window of 1° × 1°. Then, for each possible eddy center, the algorithm searches for closed SLA contours. The outermost closed SLA contour, encircling only the considered center, corresponds to the eddy edge. This method has shown to have a lower number of false eddy detection and a better estimation of eddy diameters than the method based on the Okubo-Weiss parameter [*Chaigneau et al.*, 2008; *Souza et al.*, 2011]. Note that this method is similar to the one used by *Chelton et al.* [2011] to study the main eddy characteristics at a global scale.

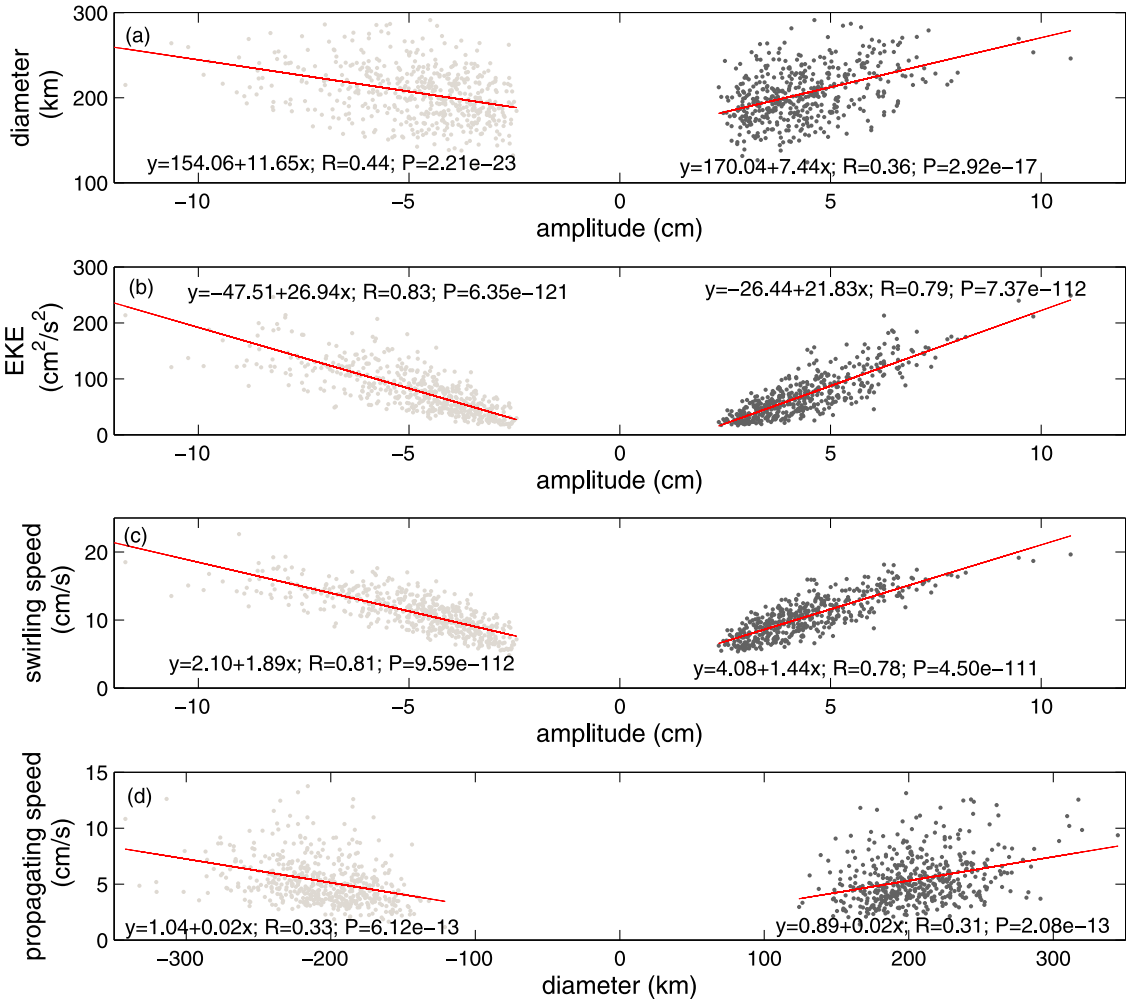

Figure 2. Comparison of different eddy properties for all eddy abundance (AEs in black; CEs in gray): (a) amplitude versus diameter, (b) amplitude versus EKE, (c) amplitude versus swirl speed and (d) diameter versus propagating speed. Red lines represent linear fits.

2.3. Eddy Tracking and Eddy Characteristics

[9] Eddies were identified in the 939 weekly SLA maps, and we only retained eddies having diameters and amplitudes higher than 80 km and 1 cm, respectively. Eddies were then separated according to their polarity and a tracking algorithm was used to follow the path of each eddy. Eddy tracking began by checking first any contour intersection between a particular eddy (e_1) at time t and any other eddy (e_2) at time $t + dt$ (dt = 1 week). If no eddy intersection was found then a search was done in a radius restricted to 100 km in time $t + dt$, assuring that the possible e_2 was not a newly generated eddy at $t + dt$ but a continuation of e_1 in time. This assurance was performed as follows: the algorithm keeps a record of all precedent eddies and their properties, which enables it to erase all subsequent eddies that intersect with any antecedent eddy, thus only non-intersecting eddies within a radius of 100 km are kept. A test was applied to those new eddies by verifying that the translation, amplitude and EKE were similar to those of the eddy being tracked. Only if the new eddy satisfied at least two of these characteristics was considered as e_2. If no eddy was found within a 100 km radius, then the same process was applied searching at time $t + 2dt$, but now at a larger radius (less than 500 km). Since eddies may also disappear between consecutive maps (in particular if they are in the gaps between satellite ground tracks [*Chaigneau et al.*, 2008]), we searched for that same eddy two weeks after its disappearance. If no e_2 was found at $t + 2dt$, e_1 is considered as dissipated.

[10] In order to analyze the most robust eddies, we only retained those that lasted more than 10 weeks. From these robust and long-lived eddies we computed the following characteristics (described in detail below): eddy center location, distance traveled, duration, diameter, propagation speed, swirling speed, EKE, amplitude, and the advective nonlinearity parameter. Each SLA map has a certain number of eddies (which we call "eddy count"), some of which generated in that particular map (that is, in that particular week) and others generated in earlier maps (thus representing a subsequent eddy). The number of newly generated eddies per map represents "eddy generation."

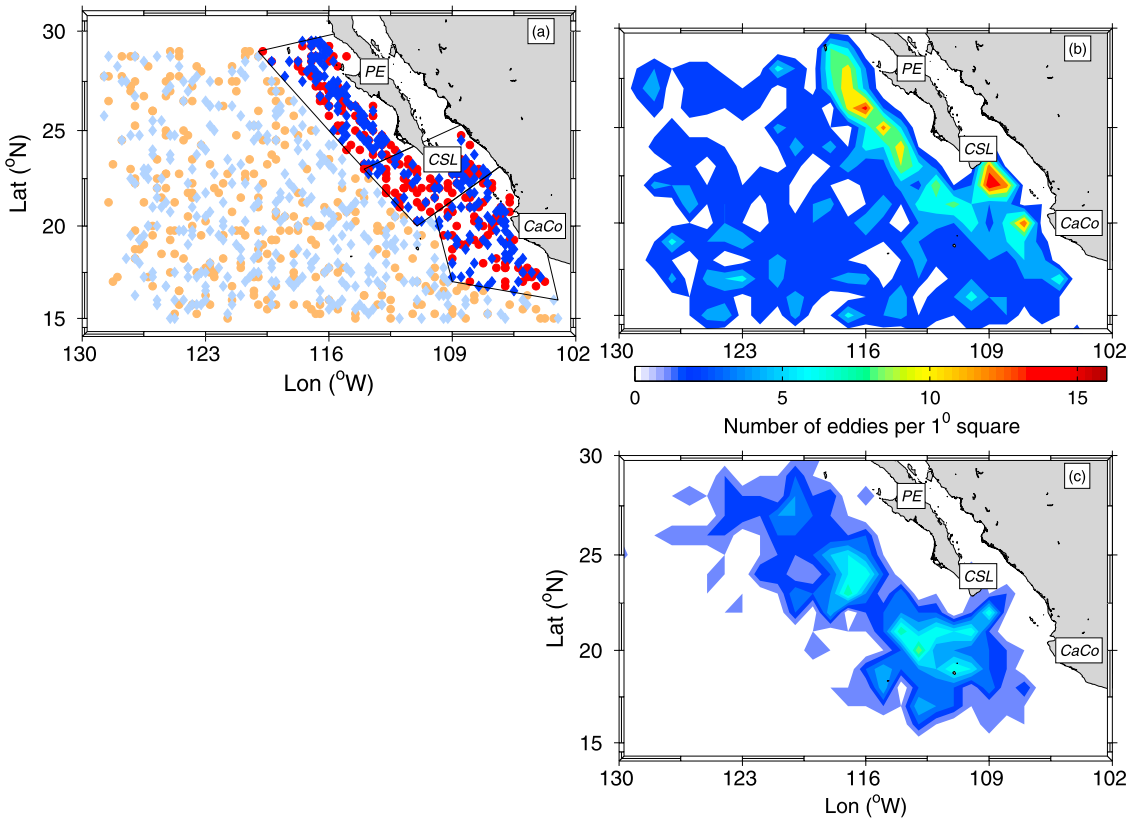

Figure 3. (a) Sites of eddy generation in the 18-year altimeter data, as seen by the SLA-B method. The polygons show the three eddy-prolific coastal areas. Coastal AE/CE eddies in red/blue, oceanic eddies are shown in light colors, respectively. (b) 1° by 1° density analysis showing where eddies were generated; red and yellow colors show the eddy-prolific areas. (c) 1° by 1° density analysis showing where coastal eddies were dissipated.

[11] Eddy characteristics were estimated as follows: Eddy center position for cyclonic or anticyclonic eddies (CEs and AEs, respectively) corresponds to the location of the minimum or maximum of SLA within the identified eddy; The duration (in days) is the total time a specific eddy is tracked; the traveled distance (km) corresponds to the total distance the eddy propagates between its birth and dissipated; the diameter (km) corresponds to the mean value between (*i*) the diameter of an equivalent circular vortex having the same area ($D = 2\sqrt{\frac{area}{\pi}}$) and (*ii*) the double of the mean value for all the radii formed between the eddy center and the eddy contour coordinates; the propagation speed (cm/s) corresponds to the ratio between the traveled distance and duration; the swirling speed (cm/s) corresponds to the mean surface geostrophic speed inside the eddy; the EKE (in cm^2/s^2) corresponds to the spatial average of the EKE within the vortex area. The amplitude (or surface displacement in cm) is the absolute difference between the SLA values at the eddy edge and eddy center (all amplitudes are positive, but we transformed cyclonic amplitudes into negative values for distinction purposes); lastly, the nonlinearity parameter of each eddy is defined as (U/c), that is, the ratio between the maximum of the geostrophic speed averages (corresponding to each one of the closed SLA contours within the eddy (U)) and the propagation velocities (c) shown at the different locations of the trajectory [*Chelton et al.*, 2007, 2011]. If this ratio is higher than 1 the eddy is considered nonlinear, which means that the eddy traps and transports fluid within its core.

2.4. Surface Geostrophic Flow Climatology

[12] To understand the possible relationship between some eddy characteristics and surface currents, we generated four quarterly mean maps of surface geostrophic flow in the study region (Figure 1). These maps were constructed using the monthly means obtained from the SLA data set plus the mean value of the geopotential anomaly relative to the 1027 kg/m^3 isopycnal (which in average represents a depth of ~540 m). The latter was obtained from the high-resolution (1/4°) World Ocean Atlas 2001 (WOA01) [*Boyer et al.*, 2005], distributed by the National Oceanographic Data Center (http://www.nodc.noaa.gov). The chosen isopycnal (1027 kg/m^3) represents the reference level where the geopotential anomaly calculated from in situ data showed the optimum root mean square adjustment, to the geopotential anomaly provided by the SLA climatology the WOD01 data [*Godínez et al.*, 2010].

2.5. Coastal Upwelling Index

[13] The relationship between the monthly eddy generation and some local-scale effects, such as wind speed/direction (traduced in upwelling strength) were analyzed using the

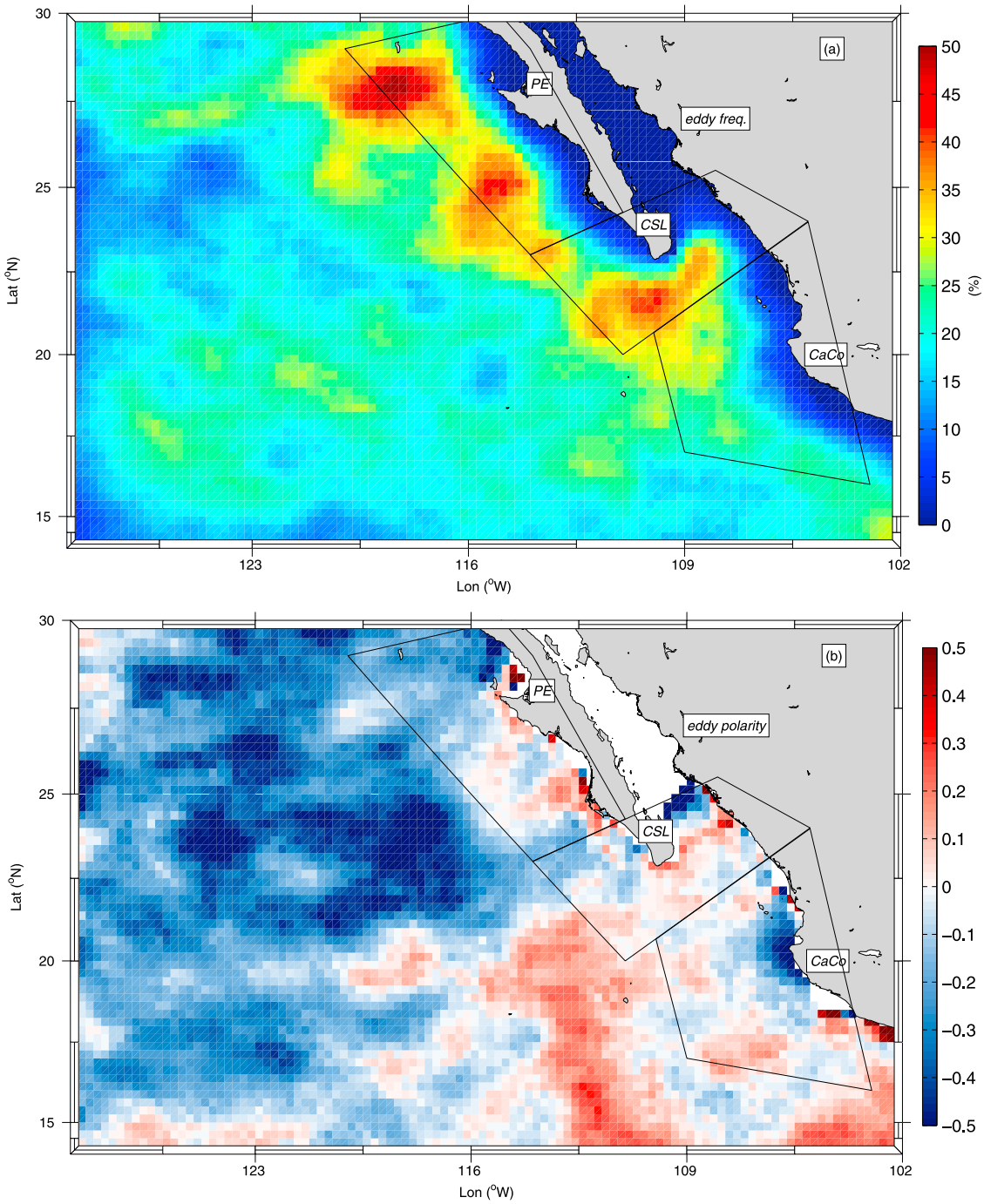

Figure 4. (a) Eddy frequency (in percentage % of weeks that a SLA pixel lies inside an eddy). (b) Eddy polarity (% of weeks that a SLA pixel lies inside a negative or positive eddy). In blue are CEs; in red are AEs.

Coastal Upwelling Index (CUI, source http://www.pfeg.noaa.gov/products/PFEL/modeled/indices/PFELindices.html), for three different locations: (1) 27°N and 116°W, in the Punta Eugenia subregion, (2) 24°N and 113°W, in the Cabo San Lucas subregion and (3) 21°N and 107°W, in the Cabo Corrientes subregion. We compared the phase of the peaks (annual and semiannual) from the climatological CUI against the phase of the peaks of the seasonal variability of eddy generation, for each coastal subregion.

3. Results

3.1. General Results

[14] Considering only eddies having a diameter ≥80 km, an amplitude ≥1 cm and a lifetime ≥10 weeks, a total of

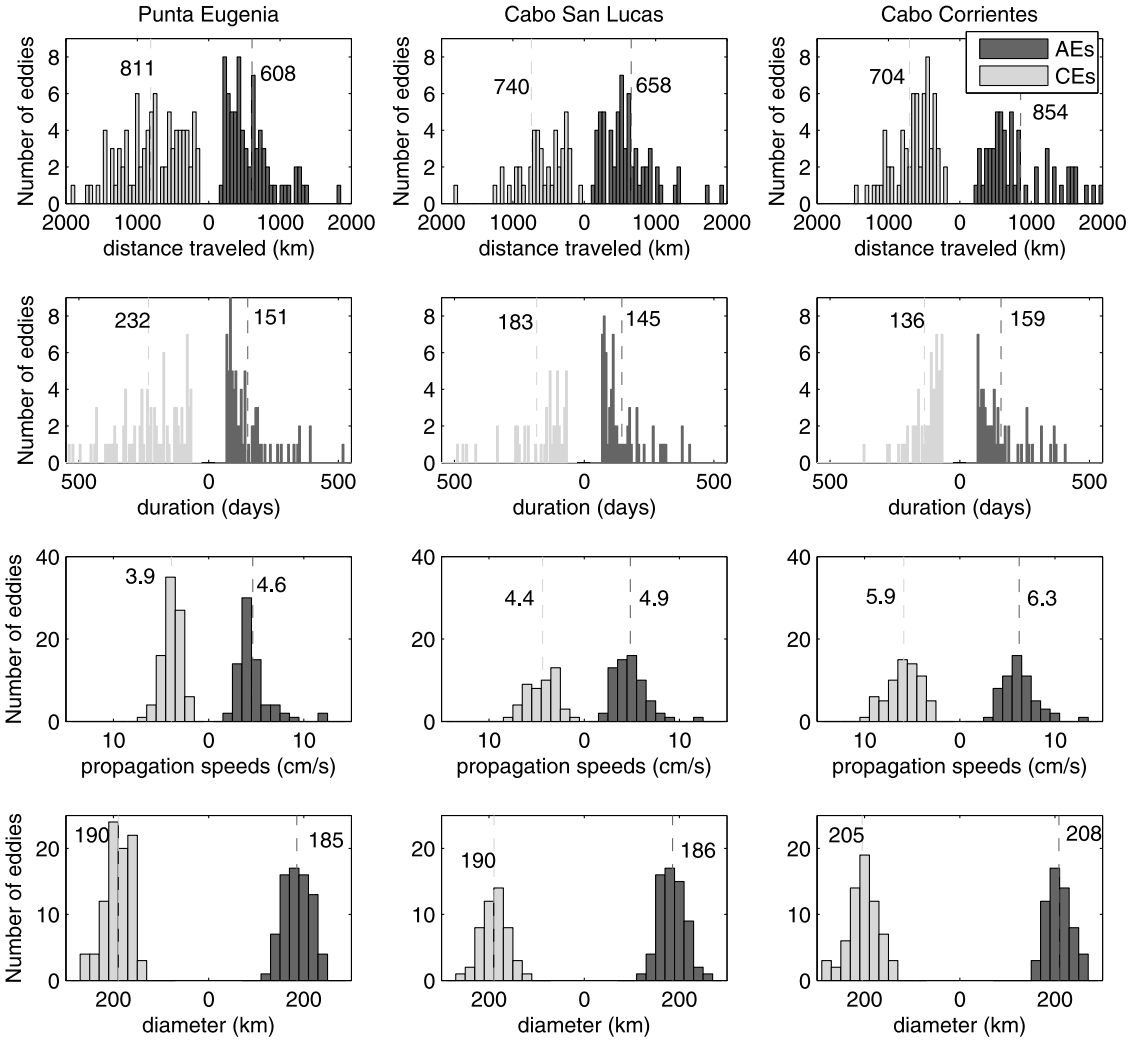

Figure 5. Histograms showing the 95% distribution and mean values (dashed line) of the distance traveled, duration, propagation speed, and diameters for the three subregions. Cyclonic distributions are shown to the left of zero.

∼8900 AEs and ∼11500 CEs were detected, corresponding to ∼500 individual trajectories of both eddy types (Table 1). In the whole study region, there is thus a preference for long-lived cyclonic eddies with ∼30% more detected CEs than AEs, and ∼15% more CE trajectories (Table 1). The difference of percentage is explained by the longer duration of CEs compared to AEs for similar propagation speeds (Table 1).

[15] The mean diameter, EKE and swirling speed as functions of the amplitude for each eddy show significant linear trends (Figures 2a–2c), demonstrating that as amplitude grows so do the diameters of eddies, their EKE and their swirling speeds. The highest correlation values, although probably overestimated due to a possible non-independence between the variables, are observed for EKE and swirling speeds, while the estimated diameters are more disperse. Figure 2d shows the corresponding growing trend between the mean eddy diameters and their propagating speeds, which is an interesting result that shows that there is a trend for larger eddies to travel faster.

3.2. Spatial Distributions

[16] The spatial distribution of eddy generation (Figure 3a) shows that eddies can be generated anywhere in the region, at least once in the 18 years. Figure 3b shows the geographical distribution of eddy genesis, corresponding to the number of initial points of eddy tracks within boxes of $1^\circ \times 1^\circ$. Eddies are preferentially generated in three near-coastal areas (polygons shown in Figure 3a) and propagate offshore before being dissipated some 480 km from the coast. Figure 3c shows where eddies generated inside these polygons (which we will call coastal eddies) were dissipated.

[17] To investigate in more detail eddy characteristics and variability, the study region was divided into the 3 near-coastal prolific subregions (marked by polygons in Figure 3a): 1.- Punta Eugenia (PE), located at the middle of the Baja California Peninsula and mainly influenced by the California Current system; 2.- Cabo San Lucas (CSL), located at the tip of Baja California peninsula and influenced by a mixture of the tropical branch of the California Current and the currents at the entrance of the Gulf of California,

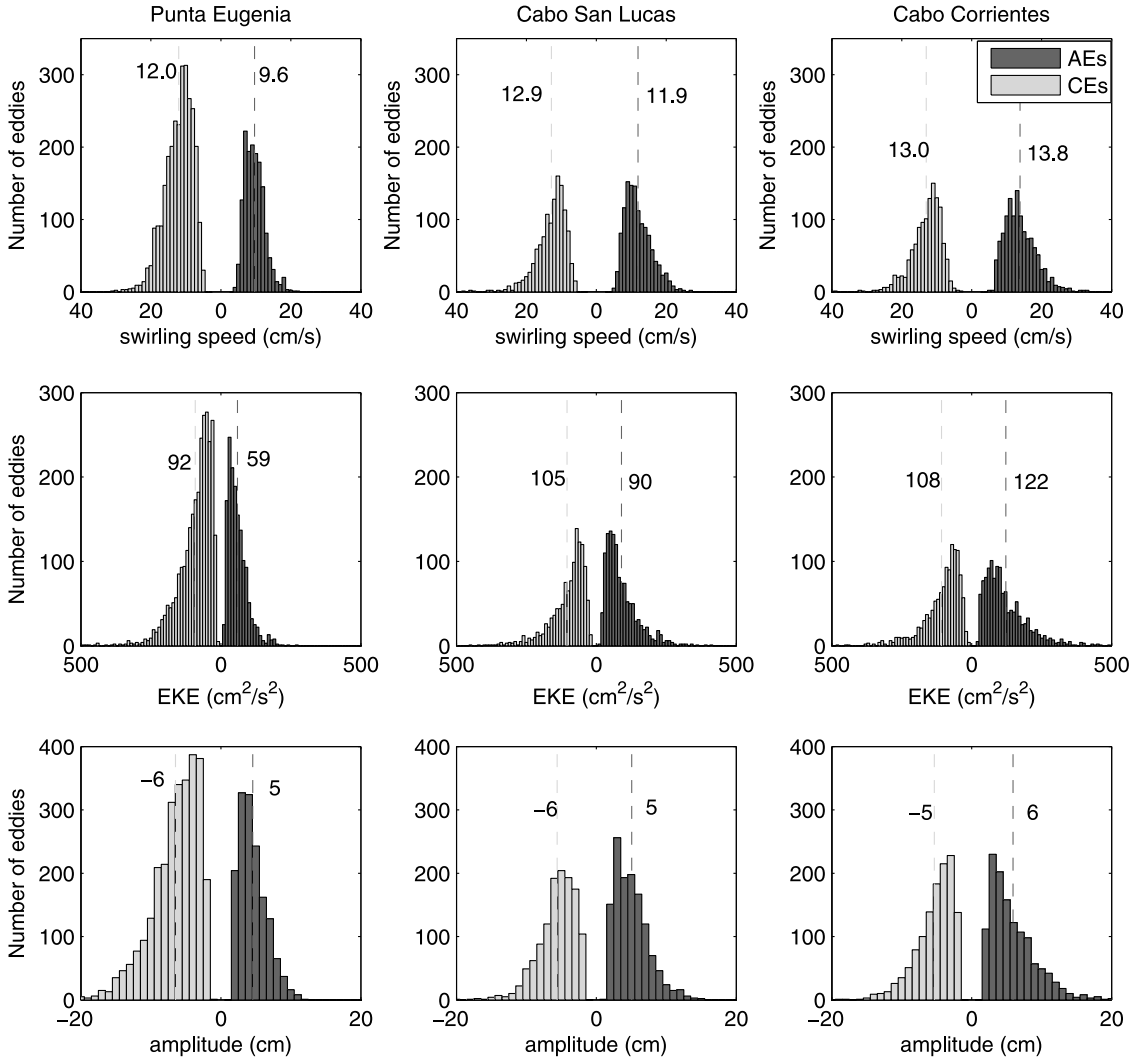

Figure 6. Histograms showing the 95% distribution and mean values (dashed line) of the swirling speed, EKE and amplitude (surface displacement) for the three subregions. Cyclonic distributions are shown to the left of zero.

including the Mexican Coastal Current; 3.- Cabo Corrientes (CaCo), located off mainland Mexico, largely influenced by the Mexican Coastal Current in summer and autumn and by the passage of coastally trapped waves.

[18] Figure 4a shows the eddy frequency distribution (EF = EF_{AEs} + EF_{CEs}), which represents, at every location, the percentage of time that the point is located within a vortex [e.g., *Chaigneau et al.*, 2008, 2009]. Relatively high EF values (up to 50%) are found in the PE and CSL subregions approximately 100 km offshore. In contrast relatively low EF values are found in Cabo Corrientes, probably associated with higher eddy propagation speeds in this subregion (Table 1 and Figure 5 (third row)). As previously noted by *Chaigneau et al.* [2008], the low EF values are related to the SLA-B algorithm, which fails to identify closed SLA contours with a diameter smaller than 80 km, close to the coast.

[19] To evaluate if there is any preference for AEs or CEs in any of the subregions, Figure 4b shows the eddy polarity (EF_{AEs} − EF_{CEs})/(EF_{AEs} + EF_{CEs}), which represents the probability of a point to be preferentially within a CE (negative polarity) or AE (positive polarity) [e.g., *Chaigneau et al.*, 2009]. In the PE subregion eddy polarity was negative at the north and slightly positive at the south. In CSL, there was also a preference for AEs indicated by a slightly positive eddy polarity. Finally, CaCo showed a marked negative polarity near the coast.

Table 2. Eddy Mean Annual Generation (Number of Eddies)[a]

Eddy Mean Annual Generation		
Whole Region	AEs	25 ± 4(31,36)
	CEs	29 ± 4(36,23)
Punta Eugenia	AEs	*4 ± 2(9,1)*
	CEs	*5 ± 2(8,2)*
Cabo San Lucas	AEs	3 ± 2(6,0)
	CEs	3 ± 1(4,1)
Cabo Corrientes	AEs	3 ± 1(5,2)
	CEs	4 ± 2(7,1)

[a]Italicized are the highest values for the coastal subregions. Maximum and minimum values are in brackets.

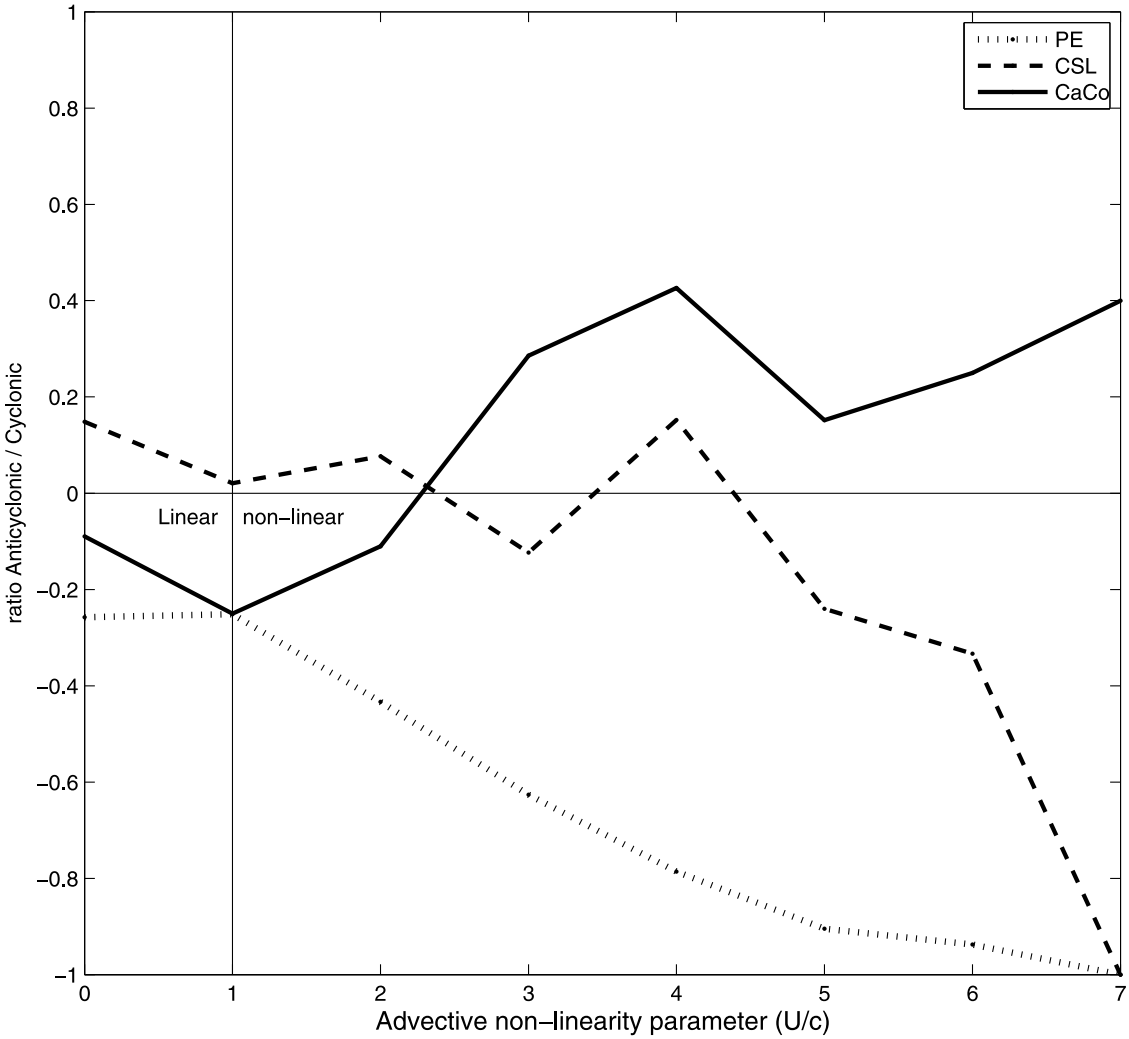

Figure 7. Ratio of the advective nonlinearity parameter (U/c) for the different locations. $U/c \geq 1$ represents nonlinear eddies. Positive (negative) values show where AEs exceed (are less) in number the quantity of CEs with the same nonlinearity value.

[20] The statistics of the main properties estimated for CEs and AEs (Figures 5 and 6), quantify the differences among the subregions; mean values, standard deviations, maxima and minima are given in Tables 1. CEs increased their distance traveled (by 13%) and duration (by 41%) from south to north (Figure 5). In contrast AEs increased their distance traveled (by 28%) and duration (by 5%) from north to south. In PE, there were more CEs than AEs generated (Table 1) but the higher duration time and weaker propagation speeds of AEs in this region (Figure 5, first and third rows) are responsible for a positive polarity in the south of PE (Figure 4b). In CSL, more AEs than CEs were generated (16% more), but we found a small difference in the total eddy count (5% more AEs) due to the higher duration of cyclones (21% more days). In CaCo there were more CEs than AEs generated, but in contrast to CSL, there was a higher number of AEs in the total count (2% more) because AEs last longer than CEs (15% more). Care should be taken when analyzing the results of the study region as a whole, because the differences between the coastal subregions would be masked. Regarding the whole-area eddy mean annual generation (Table 2), there were ∼14% less AEs generated than CEs. PE shows the highest production, followed by CaCo and CSL. For both types of eddies the propagation speed, diameter, swirling speed and EKE increased southward from PE to CaCo (Figure 6). In all the subregions, AEs tended to travel faster than CEs (Figure 5, third row): 15% faster in PE, 10% faster in CSL and 6% in CaCO. This feature was explained theoretically by *Cushman-Roisin et al.* [1990] (their Figure 1).

[21] We carried out a nonparametric Mann-Whitney U test [*Sokal*, 1981; *Zar*, 1996] to test the null hypothesis that AEs and CEs came from the same population (i.e., have the same median) or not. For the whole study area as well as for each subregions, all AEs and CEs characteristics were statistically different, even though they can be numerically similar (Table 1).

3.3. Advective Nonlinearity

[22] One of the main objectives in studying mesoscale eddy activity is to understand the interaction of these structures with the mean large-scale surface circulation, such as

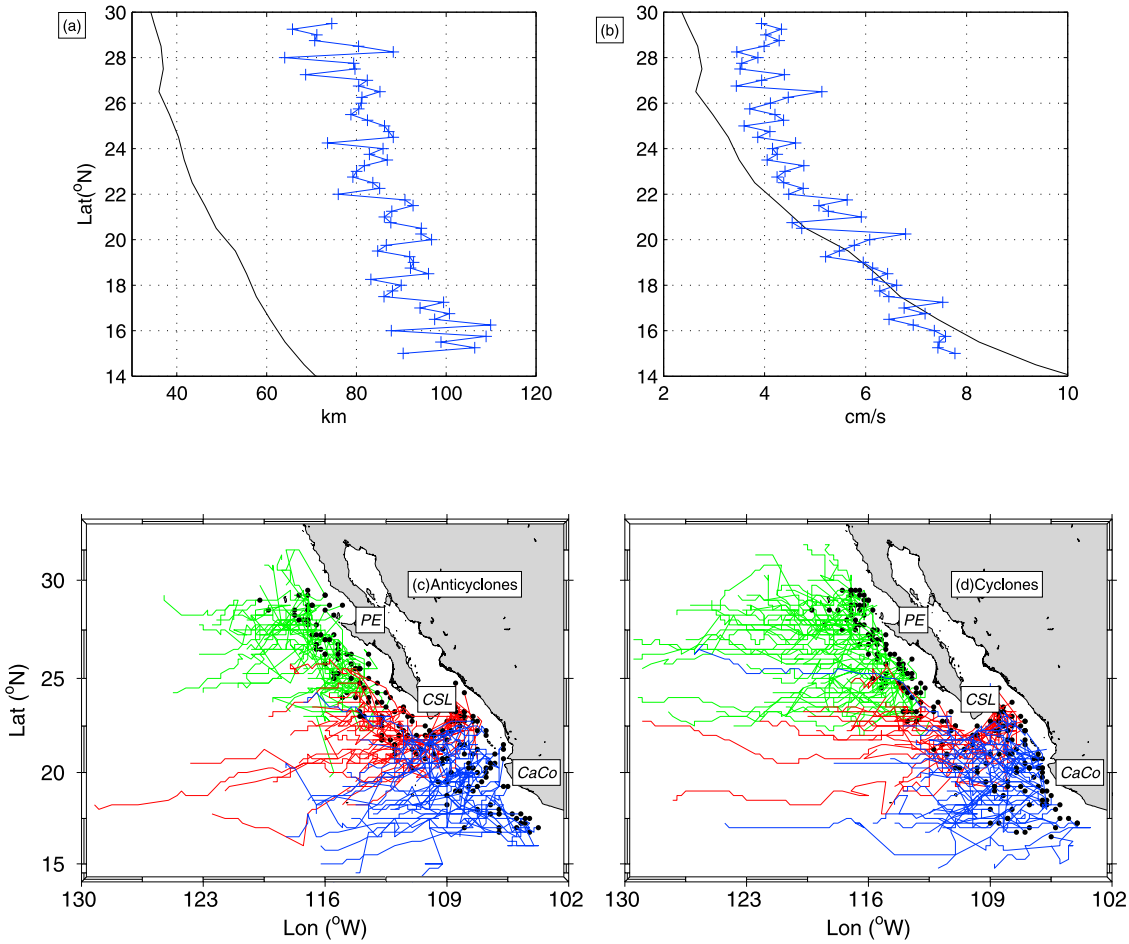

Figure 8. (a) Meridional variation of the mean zonal eddy radii and (b) propagation velocities from the SLA-B method (blue line), against the merdional variations of the Rossby radius of deformation (black line) and zonal phase speed of the first baroclinic mode Rossby waves, respectively. Tracks followed by all (c) AEs and (d) CEs generated in Punta Eugenia (PE, green lines), Cabo San Lucas (CSL, red lines), and Cabo Corrientes (CaCo, blue lines). Dots show sites of generation.

their capability of transferring water properties from the place they are generated to the site where they dissipate. The advective nonlinearity parameter (U/c) is an important measure of this capability, where U is the maximum rotational speed of the eddy and c its propagation speed, estimated at each point along the eddy trajectory. If this ratio is ≥1, eddies are considered nonlinear and this implies that the eddy cannot be regarded as a linear wave disturbance propagating through a nearly stationary medium, but instead is capable of modifying the medium as they can transfer heat, salt, carbon, nutrients, and other tracers, which can affect phytoplankton and zooplankton populations [*Chaigneau et al.*, 2011; *Chelton et al.*, 2007, 2011].

[23] For the whole study region 91.5% of long-lived eddies were nonlinear, with 25% showing a nonlinearity value ≥3, and 2% a value ≥5. In PE (Figure 7), CEs showed higher nonlinear values, probably associated with higher swirling speeds and lower propagation speeds (see also Table 1). In contrast in CaCo, AEs eddies showed higher nonlinearity than CEs and also their mean rotational speed were 7% higher. Finally, CSL showed almost the same nonlinearity (between 1 and 4) for AEs and CEs, but the higher values were preferentially associated to CEs (Figure 7). All subregions showed a similar quantity of linear eddies (∼6% of their total eddy count).

3.4. Eddy Trajectories

[24] The meridional variations of the mean zonal radii (Figure 8a) and propagation speeds (Figure 8b) of the detected eddies were compared to the meridional variation of the Rossby radius of deformation (R_d) and the zonal phase speeds of nondispersive baroclinic first-mode Rossby waves [*Chelton et al.*, 1998]. We note a southward increase of eddy diameters and propagating speed (see also diameters and propagation speeds in Table 1) which is in agreement with the meridional variation of the Rossby radius of deformation and Rossby wave speed. *Willet et al.* [2006] showed that in the case of mesoscale eddies (and after making several assumptions), the Rossby number ($R_o = U/fL$), can be expressed as $R_o = (R_d/L)^2$, where L is the scale of the eddy radius. A small R_o occurs for scales large compared to R_d, so in the case of large eddies ($L \gg R_d$), the use of the geostrophic approximation to estimate the fluid velocity in the eddy interiors from the SLA field is justified. The mean

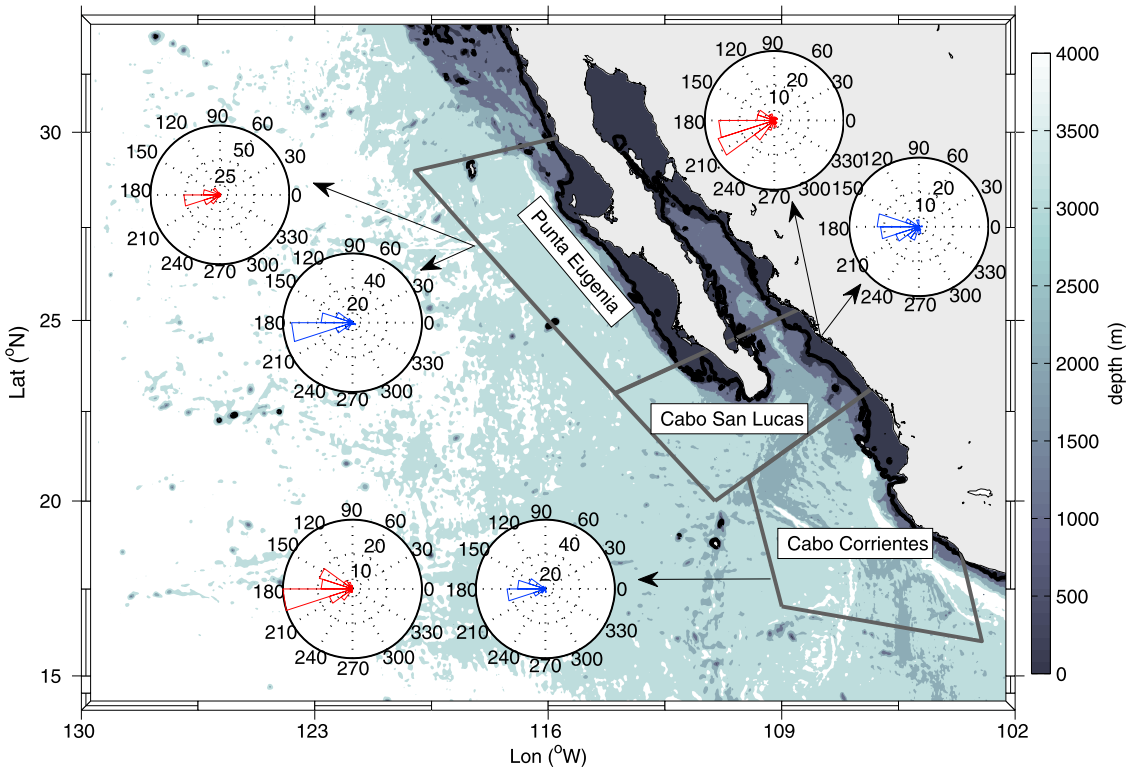

Figure 9. Bathymetry of the study region with rose diagrams for AEs (red) and CEs (blue) trajectories, for each eddy-prolific coastal subregion.

zonal radii of eddies were larger than R_d, and the mean zonal propagation of eddies were slightly faster (slower) than Rossby waves north (south) of ~19°N.

[25] Eddy trajectories generated in the three eddy-prolific locations are shown in Figures 8c and 8d and reveal that no coastally generated eddies reached the westernmost limit of our study area (130°W). As already mentioned, if the maximum rotational speed (U) of these eddies is faster than its propagation speed (c) eddies can trap fluid and advect it as they travel. 75% of the long-lived AEs/CEs propagate for more than 466/575 km in Punta Eugenia, 459/450 km in Cabo San Lucas and 728/450 km in CaCo, but particular eddies can reach larger travel distances (see maximum values in Table 1). These spatial areas were also depicted in light blue color in Figure 3c. These eddy trajectories suggest that CEs traveled further to the interior ocean than AEs, except for AEs in CaCo, which traveled larger distances (as already mentioned in section 3.2).

[26] Eddy trajectories with southward deflection, purely zonal (0° ± 1°), and with northward deflection are shown as rose diagrams in Figure 9; almost all eddies in all subregions showed a preference to travel southwest, although CEs show a higher tendency to travel northwest than AEs. In CaCo there was a higher preference for eddies to deflect northwest, in comparison with the other subregions, probably due to the advection of mesoscale eddies by the Mexican Coastal Current. All subregions show very few eastward eddy trajectories, which occurred more frequently in CSL.

[27] The bottom topography (Figure 9) offshore from the altimeter-detection and eddy generation areas does not present any major features such as troughs or ridge; therefore it did not seem to affect the eddy trajectories. Hence their traveling paths are affected only by the β-effect, reflecting a Rossby wave behavior by traveling toward the SW and NW (as shown in Figures 8c, 8d and 9).

3.5. Seasonal Variation of Eddy Generation

[28] The climatology of eddy generation in the 3 subregions was computed as the cumulative sum of the total number of generated eddies per month over the 18-year period (Figure 10). The maximum AE (CE, respectively) generation occurs in June (April) in PE, in September (December) in CSL, and in October (April) in CaCo. Superimposed to the bars of the seasonal variation is the annual plus the semi-annual components of eddy generation (seasonal fit, lines in Figure 10a–10c): PE shows a very strong annual variability for CEs (69% annual, 5% semi-annual of the total explained variance (EV)) and a strong seasonal variability for AEs (25% annual, 19% semi-annual of EV), the seasonal fit lines also show that AE and CE productions are in phase. CSL shows a strong semi-annual variability for both AEs (3% annual, 43% semi-annual of EV) and CEs (1% annual, 73% semi-annual of EV), but AE and CE productions are out of phase. Finally CaCo shows a strong seasonal variability for AEs (24% annual, 16% semi-annual) and a strong semi-annual variability for CEs (3% annual, 29% semi-annual of EV), with a 3-month lag approximately, between AE and CE production. Considering eddy production by quarters (Table 3) the greatest eddy production was found during spring (from April to June) in PE, and during summer (July to September) in CSL and CaCo.

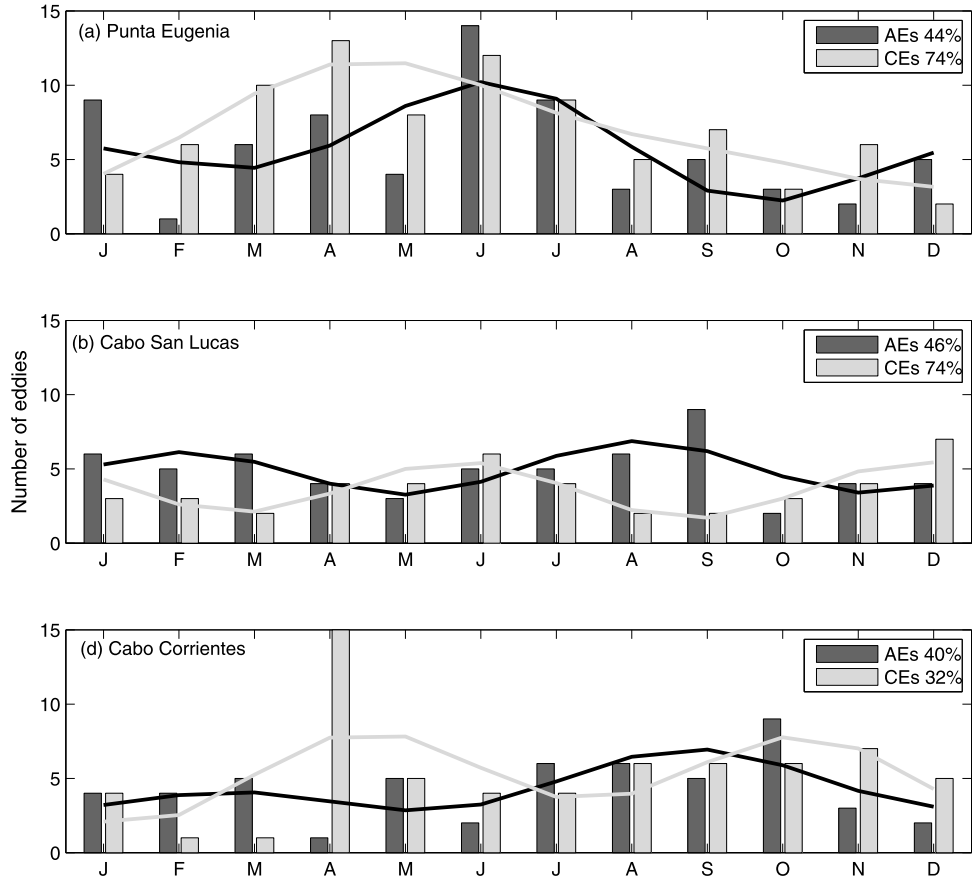

Figure 10. Bars show the cumulative sum of total eddy generation, and black/gray lines show the seasonal harmonic analysis (for AEs/CEs, respectively). The percentage represents the total variance explained by the seasonal variability (annual plus semi-annual), for the three subregions.

3.6. Interannual Variability of Eddy Generation

[29] The possible relation of the El Niño/Southern Oscillation (ENSO) phenomenon with the generation of eddies was studied by correlating different ENSO climate variability indices with monthly eddy generation for each subregion. Although correlations were significant, they were very low ($r < 0.15$), which means that most of the eddy generation variability was not related to ENSO. The annual eddy generation and its anomalies (Figure 11), for each subregion, showed a different behavior in the generation of eddies (AEs or CEs) with no clear influence of ENSO, neither in the warm nor cold phase. In our time series there are two warm (1991–1993 and 1997–1998) and two cold (1999–2001 and 2007–2008) events. Looking at the cumulative sum of annual eddy generation for the three subregions (Figures 11a–11c), there is a peak in 1999 and a drop in 1997–98 (1996 in CaCo). However, when we analyzed the anomalies of eddy generation for each subregion

Table 3. Percentage of the Total Number of Eddies Generated by Quarters[a]

		Percentage of Eddies Generated			
Coastal Location		Spring	Summer	Autumn	Winter
Punta Eugenia	AEs	38%	25%	14%	23%
	CEs	39%	24%	13%	24%
	total	*63 eddies*	*40 eddies*	*22 eddies*	*38 eddies*
Cabo San Lucas	AEs	20%	34%	17%	29%
	CEs	32%	18%	32%	18%
	total	*29 eddies*	*31 eddies*	*26 eddies*	*28 eddies*
Cabo Corrientes	AEs	15%	33%	27%	25%
	CEs	38%	25%	28%	9%
	total	*34 eddies*	*36 eddies*	*35 eddies*	*20 eddies*

[a]Total = AEs plus CEs number of eddies generated.

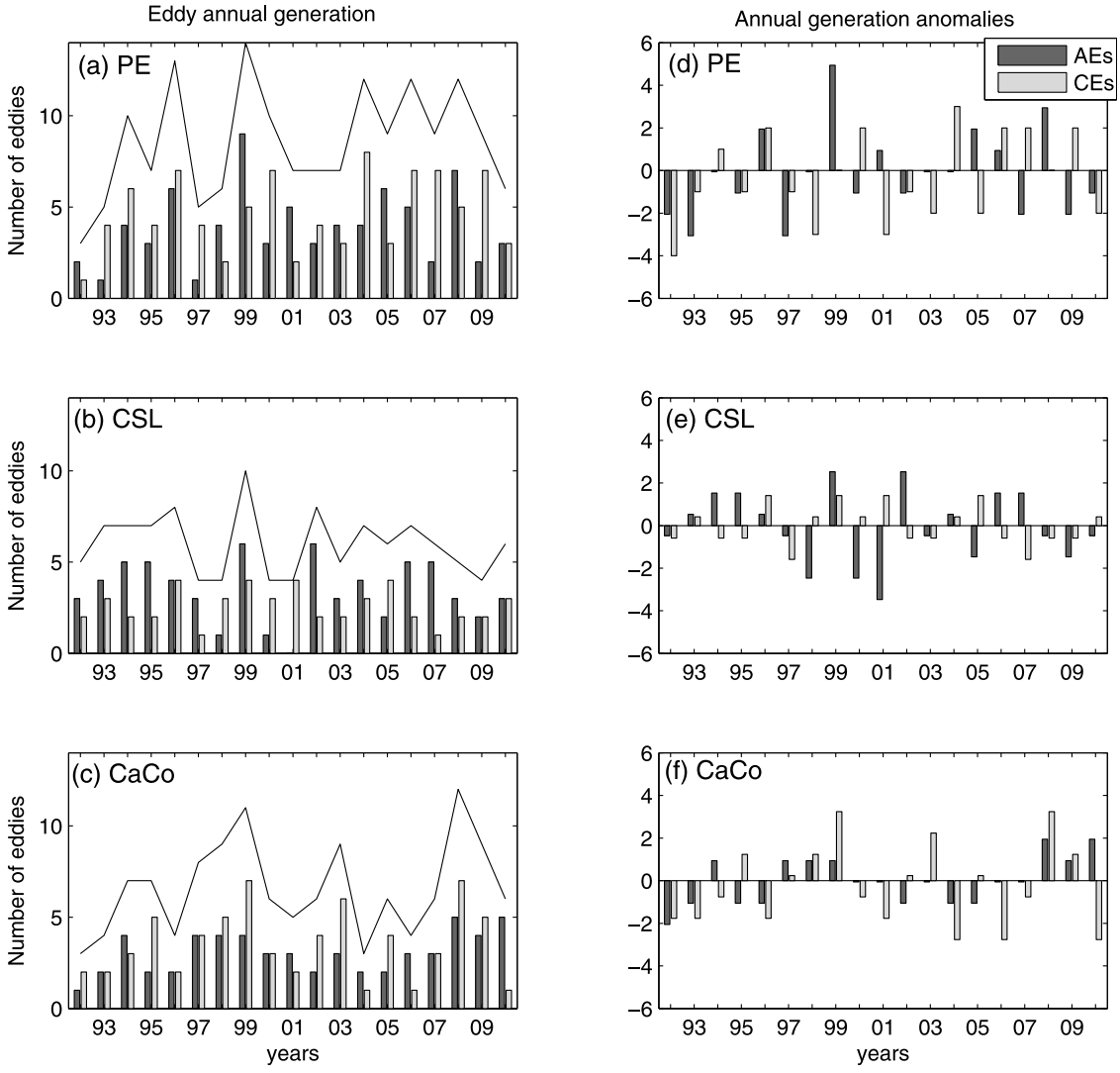

Figure 11. Bars show (a–c) the annual eddy generation and (d–f) their anomalies, for the different locations. Solid line (in Figures 11a–11c) shows the cumulative sum (AEs + CEs) of eddy generation.

(Figures 11d–11f) we found that there was no clear pattern of how ENSO events affect eddy generation, since it can rise or decrease in either phase (Table 4).

4. Discussion

[30] Based on 18 years of altimeter merged data (October 1992–October 2010), we investigated the characteristics of mesoscale activity in the NE Pacific tropical-subtropical transition zone. Eddies that lasted more than 10 weeks were preferentially generated in three near-coastal regions, where the coastline orientation changes abruptly: Punta Eugenia, Cabo San Lucas and Cabo Corrientes. Eddy characteristics were significantly different in these three areas, which indicates that care should be taken when applying results of analysis from large ocean areas since important local differences will be masked.

[31] The seasonal signal of eddy generation (Figure 10) contains annual and semiannual frequencies of similar importance, which is reflected in its bimodal structure. Since the seasonal variability of eddy generation can be related to physical forcings, we investigated the relationships between the seasonal signal of eddy generation with: (i) the large-scale geostrophic flow (Figure 1), considering that surface currents and their associated vertical shear can be favorable to eddy production, and (ii) nearshore surface winds as represented by the Coastal Upwelling Index (Figure 12), since the wind can alter the baroclinic structure of coastal areas by inducing instabilities and by coastal current intensification. These two forcings are not completely independent, but they can be analyzed separately because, e.g., the offshore California Current is part of the North Pacific Gyre, which is in Sverdrup balance with the large scale winds, but

Table 4. Influence of ENSO Events on Eddy Generation

	Warm Phase (El Niño)		Cold Phase (La Niña)	
	1991–93	1997–98	1999–01	2007–08
Punta Eugenia	decreased	decreased	raised AEs	raised AEs
Cabo San Lucas	raised	decreased AEs	raised CEs	decreased CEs
Cabo Corrientes	decreased	raised	decreased	raised

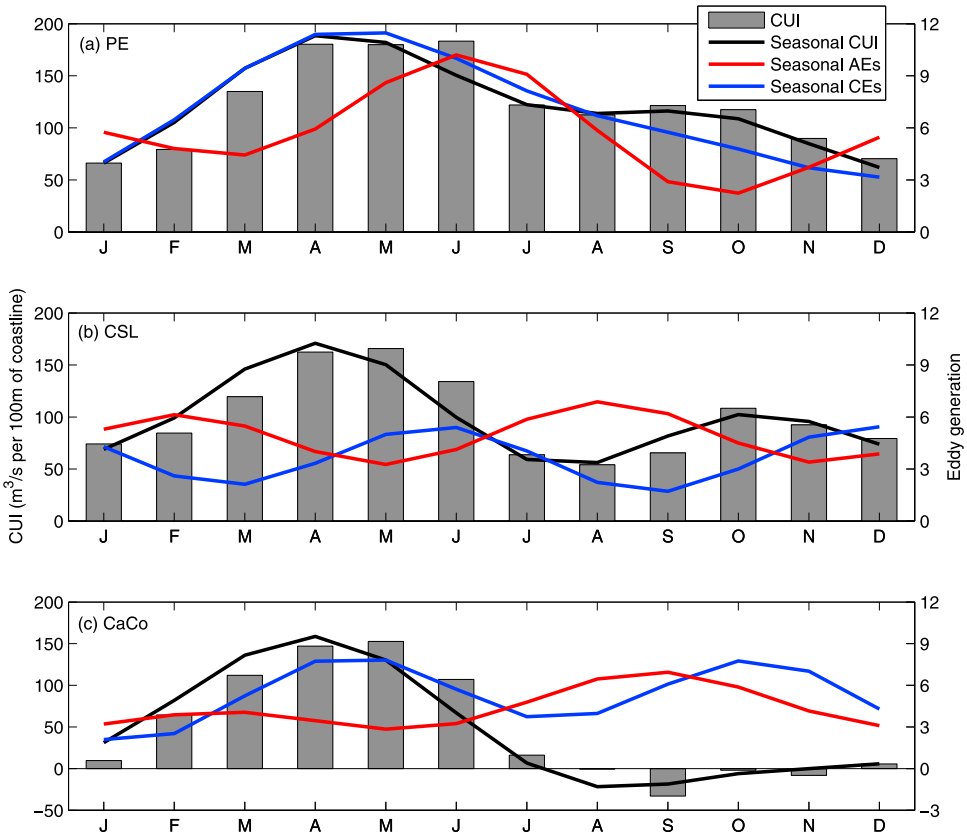

Figure 12. Bars show the climatological the monthly Coastal Upwelling Index (CUI), and the black line is its seasonal variability. The seasonal variability of AEs is in red and of CEs is in blue. (a) Punta Eugenia subregion. (b) Cabo San Lucas subregion. (c) Cabo Corrientes subregion.

the seasonal signal of the coastal winds also affect it, through inshore current enhancement and vertical mixing by coastal upwelling.

4.1. Relationships With Climatological Surface Currents and Upwelling

[32] In the case of PE the high proportion of variance explained by the seasonal signal (Figure 10a) suggests a seasonal forcing. The surface currents offshore of PE are seasonal, with maximum in spring (Figure 1a) but also strong in summer, which coincides with the maximum eddy production (61 eddies, Table 3); in late spring for CEs and early summer for AEs. The maximum of CEs production in May and AEs in June may be related to the CUI maximum in April (Figure 12a). As Figure 3b indicates, the highest count of eddies generated (16 eddies in the 18 years) occurred to the south of the abrupt change in the coastline.

[33] In CSL, the variability of generation for both, AEs and CEs, is strongly semi-annual (Figure 10b) with the maxima in CE generation in June and December and those of AEs in February and August. The summer maximum in AE production could be related with the intensification of the Mexican Coastal Current and the strong circulation in the entrance of the Gulf of California (Figure 1b). The AE production maximum in winter can be related with the strong currents at the entrance of the Gulf of California (Figure 1d). The maxima in CE generation in June and December could be related to the maximum CUI in April and October (Figure 12b). From Figure 3b, the highest count of eddies (16 eddies) was at the entrance of the Gulf of California, where the coastline changes abruptly.

[34] In CaCo, the production of AEs is annual (Figure 10c), with maximum in September, which coincides with the summer maximum strength of the Mexican Coastal Current (Figure 1b). The generation of CEs is semi-annual (Figure 10c); the May maximum may be related with the April CUI, and that in October with the end of the maximum of the Mexican Coastal Current (Figure 1c) and the downwelling conditions in September (Figure 12c). Figure 3b shows the highest eddy count (14 eddies) to the northwest of the abrupt change in the coastline.

4.2. Comparison With Hydrographic Observations

[35] *Lynn and Simpson* [1987] and *Durazo and Baumgartner* [2002] indicated that the bight north of PE (Bahía Vizcaíno) is an area of AE generation. Our eddy polarity result (Figure 4b) corroborates the AE preference in this region, although Table 1 shows that for the wider PE subregion there are slightly more CEs generated than AEs; however, our study deals only with long-lived eddies which may explain the observed difference. Our map of preferred eddy generation areas (Figure 3b) shows that the corresponding eddy-prolific area is seaward of Bahia Vizcaíno, possibly due to the poor resolution of the altimeter data near the coast. Analyzing observations from 11 oceanographic surveys conducted between 2000 and 2002

(approximately one cruise every 3 months) in the California Current area off the Baja California peninsula, *Soto-Mardones et al.* [2004] reported that summer brought a period of eddy generation while in spring no eddies were formed but only meanders. In contrast, our results show that the highest long-lived eddy formation in PE occurs during spring with 39% of the total eddy generated for this subregion; we identified summer as the second highest eddy formation seasons (see Table 3) with 25% of total eddy generation. From their short period of study (2000–2002, reported as La Niña conditions), *Soto-Mardones et al.* [2004] also suggested that off PE eddies tended to be mostly cyclonic. On the other hand from the results of annual anomalies of eddies generated (Figure 11a) we found a greater production of CEs in 2000 and a greater production of AEs during 2001. However, our polarity results corroborate the cyclonic preference off PE. Based on a single AE observation near PE, *Soto-Mardones et al.* [2004] reported a propagation speed and diameter of 4.0 cm s^{-1} and 120 km, respectively, in the range of the property values shown in Table 1.

4.3. Comparison With Numerical Models and Other Eddy Detection Results

[36] From numerical model simulations, *Zamudio et al.* [2007] proposed that in CSL and CaCo regions, mean poleward local currents driven by local wind-forcing are intensified by the passage of equatorial baroclinic coastally trapped waves, and generate both AEs and CEs near cape-like features of the coastline or shelf break; these suggestions are supported by our identification of these two areas as eddy-prolific locations (Figure 3b). On the other hand they reported that the coastally trapped waves solely have a mean annual generation (from 1979 to 2001) of 2.35 and 2.5 AEs for CaCo and CSL, respectively. In our case we found a similar mean annual generation of 3 AEs for both subregions. Although the numerical model of *Zamudio et al.* [2007] did generate cyclones, they argued that they were rapidly dissipated by the coastally trapped waves, and due to entrainment problems they were unable to resolve cyclonic eddy dynamics correctly. In our case we found a mean annual generation of 3 CEs for CSL and 4 for CaCo. In Table 1 we show that CEs in CSL lasted longer (21%) and traveled further (11%) than AEs, although there were more AEs generated (25% more). In CaCo there were more CEs generated (13% more), but AEs lasted longer (13%) and traveled farther (18%). As mentioned above, the differences between their model and our AEs observations could be attributed to the different methods employed to detect and count eddies as well as estimate their properties. Also, these authors only reported the mean annual generation of AEs due to coastally trapped waves, ignoring the other physical forcings. *Zamudio et al.*, [2007] also reported some mean AE characteristics for both subregions: a radius of ∼50 km, amplitude of ∼15 cm, and a swirl speed of ∼45 cm s^{-1}. This radius is much smaller than our observations whereas the modeled eddy amplitudes and swirling speeds are much higher. Again we believe that these differences are due to the differences in methodology, also it is worth mention that the altimeter SLA fields are overly smoothed because of limitations in the resolution of the AVISO data set, hence real eddies in the ocean could be smaller than depicted in the smoothed AVISO SLA fields.

[37] Regarding interannual eddy variability, the numerical simulations of *Zamudio et al.* [2001] suggested that during the warm phase of the ENSO phenomenon, a strong coastal jet develops off the coasts of Central America and southern Mexico, which becomes unstable and breaks into AEs; therefore more AEs should be generated during such events. Furthermore, these authors argued that strong AEs are generated only during El Niño years (although no definition was given for "eddy strength"). In the case of CSL we found negative anomalies of eddy generation (Figure 11e) while in CaCo we found positive anomalies (Figure 11f). The time series of eddy characteristics for these two subregion (not shown) show that eddies with high EKE, swirling speed and amplitude (principally AEs in CaCo and CEs in CSL) did occur during the 1997–98 warm event, although no correlation was found between the Multivariate ENSO index (MEI) and eddy generation in both subregions. Further investigations are needed to increase our knowledge of the relationship between eddy generation and the ENSO phenomenon.

[38] From a 3-year numerical simulation (2003–2005) of the study region, *Pantoja et al.* [2012] suggested that the interaction of currents flowing south out the Gulf of California with the poleward Mexican Coastal Current produce a lateral current shear that originates baroclinic instabilities that promote the generation of eddies. The prolific area located in CSL (at the entrance of the Gulf of California, Figure 3b) is in agreement with their results, and also Table 3 shows that summer is the season with the greatest eddy generation (27% of the Total eddy generation). These authors also reported that AEs were larger and lasted longer than CEs, whereas we found that CEs last longer (21%), traveled farther (11%) and were larger (2%) than AEs.

[39] Using a year of numerical simulations (1987) of the California Current region, *Pares-Sierra et al.* [1993] concluded that the wind-driven coastal generation of mesoscale eddy activity dominates that of baroclinic instability. We found that monthly eddy generation can be related with both, surface winds (expressed as the CUI (Figure 12)) and the interactions between the strength of surface currents and coastline effects. Two other reports support this last hypothesis: (1) *Jerónimo and Gómez-Valdés* [2007], from direct hydrographic observations acquired during July 2004, observed a subsurface AE in the PE subregion and suggested that local bathymetry might trigger the development of baroclinic instabilities in the California Undercurrent, causing generation of eddies. (2) North of PE subregion (off the Californian coast), *Kurian et al.* [2011] used the Okubo-Weiss parameter to detect eddies form a 12-year run of a high-resolution climatological model, suggesting that the subsurface California Undercurrent tend to generate subsurface intensified AEs through instabilities and topographic or coastline effects.

[40] *Chelton et al.* [2011] argued that eddies are most likely formed from meanders that pinch off of the eastern boundary currents and undercurrents or from other manifestations of baroclinic instability. They observed that eddy polarity can be very inhomogeneous regionally; in the case of mesoscale variability off the coast of California, they commented that it is predominantly cyclonic on the offshore

side of the equatorward California Current, presumably due to meanders that pinch off CEs, while AEs occur on the inshore side of the California Current near major capes. Although we did not observe this eddy polarity difference between the inshore/offshore sides of the California Current we did observe a regional polarity difference between the three coastal subregions.

[41] On their study of eddy activity in four major upwelling areas, *Chaigneau et al.* [2009] found that eddies were mainly generated along the coast at some localized "hot spots" which in our study region were principally located in the southern part of the Gulf of California (~20°N) and off Punta Eugenia (~28°N). They also observed a high eddy frequency within ~600 km off the coast south of 42°N and found that the upwelling area located in the California Current system showed the strongest seasonal variation and a relatively weak interannual variability compared to the other upwelling areas. These last two results are very similar to what we found for each coastal subregion: a strong seasonal variability and a very weak interannual variation of eddy generation.

5. Conclusions

[42] Using 18 years of satellite altimetry data and the SLA-B method to automatically identify eddies, we found that there are three near-coastal eddy-prolific areas (Figure 3) in the NE Pacific tropical-subtropical transition zone: (1) Punta Eugenia in the Baja California Peninsula, (2) Cabo San Lucas at the entrance to the Gulf of California, and (3) Cabo Corrientes off central Mexico. These three areas are located in places where the coastal morphology changes abruptly and strong surface current intensification occurs at some phase of the seasonal cycle. Although mesoscale eddies in these areas have been previously reported, this study provides their first statistically supported characterization. Clear statistical differences were found in eddy properties for the three subregions: Punta Eugenia showed the highest eddy production (with more cyclones generated), followed by Cabo Corrientes (also with more cyclones) and Cabo San Lucas (with more anticyclones). Cabo Corrientes eddies showed the highest mean values in propagation speed, swirling speed and EKE, whereas Punta Eugenia eddies showed the lowest values. CEs increased their distance traveled (by 13%) and duration (by 41%) from south to north, whereas AEs increased their distance traveled (by 28%) and duration (by 5%) from north to south. In the mean, anticyclones tend to travel faster than cyclones in all the subregions, 15% faster in PE, 10% faster in CSL and 6% in CaCO. These long-lived eddies were mainly (91%) nonlinear and therefore can redistribute coastal waters relatively far into the open ocean. 75% of these AEs/CEs propagate for more than 466/575 km in Punta Eugenia, 459/450 km in Cabo San Lucas and 728/450 km in Cabo Corrientes, but particular eddies can reach larger distances. The peaks in the seasonal signal of eddy generation can be associated to peaks in the strength of the offshore currents and/or in the Coastal Upwelling Index (phase difference ~1.5 months). No clear relationship could be established between El Niño events and eddy generation.

[43] **Acknowledgments.** This is a product of project "Investigaciones Oceanográficas del Sistema Frontal de Baja California Sur" supported by CONACyT (SEP-2008-103898, PI EB). J.A.K. was recipient of a CONACyT PhD scholarship. Additional support was received from CICESE internal budget. The altimeter product were produced by *Ssalto/Duacs* and distributed by *AVISO*, with support from CNES. We would like to thank Francesco Nencioli for the advice and distribution of the Vector Geometry method, Julio Sheinbaum and two anonymous reviewers, whose expertise was very valuable for the improvement of this study.

References

Boyer, T., S. Levitus, H. Garcia, R. A. Locarnini, C. Stephens, and J. Antonov (2005), Objective analyses of annual, seasonal, and monthly temperature and salinity for the World Ocean on a 0.25° grid, *Int. J. Climatol.*, *25*, 931–945, doi:10.1002/joc.1173.

Chaigneau A., A. Gizolme, and C. Grado (2008), Mesoscale eddies off Peru in altimeter records: Identification algorithms and eddy spatio-temporal patterns, *Prog. Oceanogr.*, *79*, 106–119, doi:10.1016/j.pocean.2008.10.013.

Chaigneau, A., G. Eldin, and B. Dewitte (2009), Eddy activity in the four major upwelling systems from satellite altimetry (1992–2007), *Prog. Oceanogr.*, *83*, 117–123, doi:10.1016/j.pocean.2009.07.012.

Chaigneau, A., M. Le Texier, G. Eldin, C. Grados, and O. Pizarro (2011), Vertical structure of mesoscale eddies in the eastern South Pacific Ocean: A composite analysis from altimetry and Argo profiling floats, *J. Geophys. Res.*, *116*, C11025, doi:10.1029/2011JC007134.

Chelton, D. B., R. A. de Szoeke, M. G. Schlax, K. El Naggar, and N. Siwertz (1998), Geographical variability of the first baroclinic Rossby radius of deformation, *J. Phys. Oceanogr.*, *28*, 433–460, doi:10.1175/1520-0485(1998)028<0433:GVOTFB>2.0.CO;2.

Chelton, D. B., M. G. Schlax, R. M. Samelson, and R. A. de Szoeke (2007), Global observations of large oceanic eddies, *Geophys. Res. Lett.*, *34*, L15606, doi:10.1029/2007GL030812.

Chelton, D. B., M. G. Schlax, and R. M. Samelson (2011), Global observations of nonlinear mesoscale eddies, *Prog. Oceanogr.*, *91*, 167–216, doi:10.1016/j.pocean.2011.01.002.

Cushman-Roisin, B., E. P. Chassignet, and B. Tang (1990), Westward motion of mesoscale eddies, *J. Phys. Oceanogr.*, *20*, 758–768, doi:10.1175/1520-0485(1990)020<0758:WMOME>2.0.CO;2.

Ducet, N., P. Y. Le Traon, and G. Reverdin (2000), Global high resolution mapping of ocean circulation from TOPEX/POSEIDON and ERS-1/2, *J. Geophys. Res.*, *105*, 19,477–19,498, doi:10.1029/2000JC900063.

Durazo, R., and T. R. Baumgartner (2002), Evolution of oceanographic conditions off Baja California: 1997–1999, *Prog. Oceanogr.*, *54*, 7–31, doi:10.1016/S0079-6611(02)00041-1.

Godínez, V. M., E. Beier, M. F. Lavín, and J. A. Kurczyn (2010), Circulation at the entrance of the Gulf of California from satellite altimeter and hydrographic observations, *J. Geophys. Res.*, *115*, C04007, doi:10.1029/2009JC005705.

Guerrero, L., J. Sheinbaum, and J. Candela (2004), Tracking eddies in the Caribbean Sea using the AVISO Altimetry Analysis, paper presented at the Western Pacific Geophysics Meeting, Honolulu, Hawai'i, 16–20 Aug.

Haller, G. (2005), An objective definition of a vortex, *J. Fluid Mech.*, *525*, 1–26, doi:10.1017/S0022112004002526.

Henson, S. A., and A. C. Thomas (2008), A census of oceanic anticyclonic eddies in the Gulf of Alaska, *Deep Sea Res., Part I*, *55*, 163–176, doi:10.1016/j.dsr.2007.11.005.

Jerónimo, G., and J. Gómez-Valdés (2007), A subsurface warm-eddy off northern Baja California in July 2004, *Geophys. Res. Lett.*, *34*, L06610, doi:10.1029/2006GL028851.

Kessler, W. S. (2006), The circulation of the eastern tropical Pacific: A review, *Prog. Oceanogr.*, *69*, 181–217, doi:10.1016/j.pocean.2006.03.009.

Kurian, J., F. Colas, X. Capet, J. C. McWilliams, and D. B. Chelton (2011), Eddy properties in the California Current System, *J. Geophys. Res.*, *116*, C08027, doi:10.1029/2010JC006895.

Lavín, M. F., E. Beier, J. Gomez-Valdes, V. M. Godínez, and J. Garcia (2006), On the summer poleward coastal current off SW Mexico, *Geophys. Res. Lett.*, *33*, L02601, doi:10.1029/2005GL024686.

Le Traon, P. Y., Y. Faugère, F. Hernandez, J. Dorandeau, F. Mertz, and M. Ablain (2003), Can we merge GEOSAT Follow-On with TOPEX/Poseidon and ERS-2 for an improved description of the ocean circulation?, *J. Atmos. Oceanic Technol.*, *20*, 889–895, doi:10.1175/1520-0426(2003)020<0889:CWMGFW>2.0.CO;2.

Lynn, R. J., and J. J. Simpson (1987), The California Current system: The seasonal variability of its physical characteristics, *J. Geophys. Res.*, *92*, 12,947–12,966, doi:10.1029/JC092iC12p12947.

Morrow R., F. Birol, D. Griffin, and J. Sudre (2004), Divergent pathways of cyclonic and anti-cyclonic ocean eddies, *Geophys. Res. Lett.*, *31*, L24311, doi:10.1029/2004GL020974.

Nencioli, F., C. Dong, T. Dickey, L. Washburn, and J. C. Mcwilliams (2010), A vector geometry–based eddy detection algorithm and its application to a high-resolution numerical model product and high-frequency

radar surface velocities in the Southern California Bight, *J. Atmos. Oceanic Technol.*, *27*, 564–579, doi:10.1175/2009JTECHO725.1.

Okubo, A. (1970), Horizontal dispersion of floatable particles in the vicinity of velocity singularities such as convergences, *Deep Sea Res. Oceanogr. Abstr.*, *17*, 445–454.

Pantoja, D. A., S. G. Marinone, A. Parés-Sierra, and F. Gómez-Valdivia (2012), Numerical modeling of seasonal and mesoscale hydrography and circulation in the Mexican Central Pacific, *Cienc. Mar.*, *38*(2), 363–379.

Pares-Sierra, A., W. B. White, and C.-K. Tai (1993), Wind-driven coastal generation of annual mesoscale eddy activity in the California Current, *J. Phys. Oceanogr.*, *23*(6), 1110–1121, doi:10.1175/1520-0485(1993)023<1110:WDCGOA>2.0.CO;2.

Robinson, S. K. (1991), Coherent motions in the turbulent boundary layer, *Annu. Rev. Fluid Mech.*, *23*, 601–639, doi:10.1146/annurev.fl.23.010191.003125.

Sadarjoen, I. A., and F. H. Post (2000), Detection, quantification, and tracking of vortices using streamline geometry, *Comput. Graph.*, *24*, 333–341, doi:10.1016/S0097-8493(00)00029-7.

Simpson, J. J., and R. J. Lynn (1990), A mesoscale eddy dipole in the offshore California Current, *J. Geophys. Res.*, *95*(C8), 13,009–13,022, doi:10.1029/JC095iC08p13009.

Sokal, R. R. (1981), *Biometry: The Principles and Practice of Statistics in Biological Research*, W. H. Freeman, San Francisco, Calif.

Soto-Mardones, L., A. Pares-Sierra, J. Garcia, R. Durazo, and S. Hormazabald (2004), Analysis of the mesoscale structure in the IMECOCAL region (off Baja California) from hydrographic, ADCP and altimetry data, *Deep Sea Res., Part II*, *51*, 785–798.

Souza, J. M. A. C., C. de Boyer Montégut, and P. Y. Le Traon (2011), Comparison between three implementations of automatic identification algorithms for the quantification and characterization of mesoscale eddies in the South Atlantic Ocean, *Ocean Sci.*, *7*, 317–334, doi:10.5194/os-7-317-2011.

Strub, P. T., and C. James (2002), Altimeter-derived surface circulation in the large-scale NE Pacific Gyres. Part 1. Seasonal variability, *Prog. Oceanogr.*, *53*, 163–183.

Weiss, J. (1991), The dynamics of enstrophy transfer in two-dimensional hydrodynamics, *Phys. D*, *48*, 273–294, doi:10.1016/0167-2789(91)90088-Q.

Willet, C. A., R. R. Leben, and M. F. Lavín (2006), Eddies and tropical instability waves in the eastern tropical Pacific: A review, *Prog. Oceanogr.*, *69*, 218–238, doi:10.1016/j.pocean.2006.03.010.

Willis, J. K., D. Roemmich, and B. Cornuelle (2004), Interannual variability in upper ocean heat content, temperature, and thermosteric expansion on global scales, *J. Geophys. Res.*, *109*, C12036, doi:10.1029/2003JC002260.

Zamudio, L., A. P. Leonardi, S. D. Meyers, and J. J. O'Brien (2001), ENSO and eddies on the southwest coast of Mexico, *Geophys. Res. Lett.*, *28*(1), 13–16, doi:10.1029/2000GL011814.

Zamudio, L., H. E. Hurlburt, E. J. Metzger, and C. E. Tilburg (2007), Tropical wave-induced oceanic eddies at Cabo Corrientes and the Marıa Islands, Mexico, *J. Geophys. Res.*, *112*, C05048, doi:10.1029/2006JC004018.

Zar, J. H. (1996), *Biostatistical Analysis*, Prentice Hall, Upper Saddle River, N. J.